

Preparation of magnetic lignin-based adsorbents and its adsorption properties for dyes

J. Li, S. P. Qiu, H. F. Zhao*, D. L. Guo, Z. Y. Yan, J. H. Wu, J. Li
School of Environmental and Natural Resources, Zhejiang University of Science and Technology, Hangzhou 310023, China

In this study, the renewable magnetic lignin-based material with good properties and environmental friendliness was successfully prepared and used for the treatment of wastewater. Lignin nanospheres (LNS) were prepared from stearyl chloride esterified alkali lignin via self-assembly in the mixture and raspberry-like magnetic lignin microspheres ($\text{Fe}_3\text{O}_4@\text{SiO}_2\text{-LNS}$) was successfully prepared by grafting LNS onto the surface of $\text{Fe}_3\text{O}_4@\text{SiO}_2$ particles by chemical crosslinking, then was used as adsorbent for Methylene blue (MB) and Rhodamine B (RhB) dyes. The results indicated that the $\text{Fe}_3\text{O}_4@\text{SiO}_2\text{-LNS}$ had excellent adsorptivity in alkaline solution, and the maximum adsorption capacities for MB and RhB were $258.40 \text{ mg}\cdot\text{g}^{-1}$ and $124.38 \text{ mg}\cdot\text{g}^{-1}$, respectively. The $\text{Fe}_3\text{O}_4@\text{SiO}_2\text{-LNS}$ adsorbent can be recycled due to its good magnetism and the regeneration efficiency is over 85% after three cycles. Therefore, the prepared magnetic lignin-based adsorbent is a low-cost, high-efficiency and reusable adsorbent for wastewater treatment.

(Received June 27, 2023; Accepted August 30, 2023)

Keywords: Lignin nanospheres, Magnetic adsorbent, Methylene blue, Rhodamine B

1. Introduction

Dye is an organic compound containing chromogenic groups and autologous pigment, which has been widely used in fields of textile, printing and dyeing, papermaking and so on[1]. At present, there are more than 10 thousand kinds of industrial synthetic dyes, and the annual output is close to 7×10^5 tons, but nearly 100 tons of dyes are directly discharged into nature through wastewater every year[2]. Most of these dye molecules contain aromatic rings, which are carcinogenic, biodegradable, highly toxic and mutagenic. They not only threaten the survival of algae and fish in water, but also have a negative impact on human health through enrichment[3-5]. Therefore, how to effectively treat dyes in wastewater to obtain safe and clean production and domestic water has become an urgent environmental problem to be solved. As reported, the treatment methods of dye wastewater mainly include adsorption, membrane separation and oxidative degradation[6, 7], in which the adsorption method has the advantages of simple operation and high efficiency[8]. Several adsorbents including activated carbon, zeolite, ion exchange materials, and bentonite have been widely investigated for dye adsorption. However, due to the problems of difficulties in recovery, regeneration, reuse, high price and low adsorption efficiency, it was almost impracticable for large-scale industrial application of dye waste water treatment.

Lignin, which is the second most abundant aromatic biopolymer in nature, accounts for about 30% of organic carbon in biomass resources[9, 10]. Lignin contains a large number of functional groups including aromatic ring, hydroxyl groups, carbonyl groups, carboxyl groups, methoxy groups, and unsaturated bonds, and thus has the ability of ion exchange and adsorption. However, the industrial lignin, which was commonly separated from the pulping and papermaking process, has disadvantages of separating and recovery due to its complex chemical structure and particle diffusion properties. Based on this, lignin-based magnetic polymer adsorbent with core-shell structure has been developed rapidly in recent years. Of the abundant magnetic materials such as Fe, Co and Ni elements, alloys, oxides or composite structures, Fe_3O_4 is more widely used due to its simple preparation process, stable performance and low toxicity[11]. Li et al. dissolved aminated

* Corresponding author: zhf9966@163.com
<https://doi.org/10.15251/DJNB.2023.183.1065>

alkali lignin in concentrated ammonia water and slowly added it into the mixed solution of FeCl_3 and FeCl_2 to prepare magnetic lignin adsorbent (LAMNP) by coprecipitation[12]. Compared with ordinary alkali lignin, LAMNP is a pH sensitive adsorbent, which has better magnetic response and higher adsorption capacity, The adsorption capacity of methylene blue (MB) and Acid Scarlet GR (AS-GR) can reach $211.42 \text{ mg}\cdot\text{g}^{-1}$ and $176.49 \text{ mg}\cdot\text{g}^{-1}$ respectively. Meng et al has prepared magnetic lignin hydrogel microspheres (LDMHMs) by blending diethylenetriamine modified lignin with Fe_3O_4 particles, and used them as adsorbents for organic dyes, such as methylene blue (MB), methyl orange (MO) and malachite green (MG)[13]. Under the same conditions, the adsorption capacity of LDMHMs was higher than that of unmodified lignin, and the regeneration rate was above 90% after repeated use. Fang et al prepared magnetic lignin nanoparticles (MLN) by kraft lignin from bamboo residue and Fe_3O_4 via Mannich reaction[14]. The removal efficiency of MLN for Congo red could reach 95.5% in 30min. Kinetic modeling results showed that the adsorption process belongs to chemical adsorption of multi or mono molecular layer. Ma et al synthesized lignin-based carbon nanoparticles (MLBCN) using a precipitation-carbonization process[15]. Results showed that the adsorption of MLBCN for methyl orange was consistent with the Langmuir model and pseudo-second-order model, showing monolayer adsorption, with a maximum adsorption capacity of 113.0 mg/g and chemisorption being the rate-controlling step. Above various reports investigated on lignin-based magnetic adsorbents for treating dyes in waste water and showed the advantages of large specific surface area, quantities of surficial active sites, high adsorption efficiency and pollutant removal rate. Moreover, the adsorbent can be quickly separated from the solution through external magnetic field, thus avoid secondary pollution [16, 17]. However, the complex over-condensed non-homogeneous structure and inherent poor dispersibility of lignin still limited the adsorption performance to maximal extent.

In this study, lignin nanospheres (LNS) were firstly prepared by self-assembly through hydrophobically modification with stearyl chloride, while $\text{Fe}_3\text{O}_4@\text{SiO}_2$ was prepared by solvothermal and sol-gel method. Using chloropropyl triethoxysilane as crosslinking agent, the prepared LNS were loaded on $\text{Fe}_3\text{O}_4@\text{SiO}_2$ surface to form magnetic lignin-based microspheres used for adsorbing methylene blue (MB) and rhodamine B (RhB). In addition, the adsorption isotherm of the magnetic adsorbent for adsorbing MB and RhB were also evaluated.

2. Experimental

2.1. Materials

Alkali lignin (AL), stearyl chloride (SC), N-dimethylformamide (DMF), tetrahydrofuran (THF), triethylamine (TEA), tetraethyl orthosilicate (TEOS), chloropropyl triethoxysilane (CPTES), Ferric sulfate ($\text{Fe}_2(\text{SO}_4)_3$), ethylene glycol (EG), polyethylene glycol 4000 (PEG-4000), sodium acetate (NaAc), ammonia, n-hexane, toluene, isopropanol, Rhodamine B (RhB) and methylene blue (MB) were purchased from Macklin Biochemical Technology Co., Ltd. (Shanghai, China)

2.2. Preparation of lignin nanospheres (LNS)

AL (2.0 g) was dissolved in DMF (30 mL) and the solution was transferred to a three-mouth flask, SC (6.0 g), and TEA (2 mL) were added, and the reaction was carried out at 90°C for 7 h. After that, the obtained product was filtered and cleaned with n-hexane by Bouchner funnel. Then it was dried in a vacuum drying oven at 80°C for 24 h, and the product was esterified alkali lignin (SCAL). According to the typical self-assembly method, SCAL was dissolved in THF and prepared into 0.5 mg/mL solution, which was stirred at a speed of 1500 r/min at room temperature (25°C). At the same time, a peristaltic pump was used to slowly drop deionized water into the solution at a speed of 10 mL/min , and the dripping was stopped when the final water content was 90%. In order to quickly evaporate THF in the system, the suspension liquid containing SCAL nanospheres was continuously stirred at room temperature. After 4 h, the suspension liquid of the nanospheres were transferred into dialysis bags (M_w : 12000–14000). The residual THF in the solution was removed by dialysis. Finally, lignin nanosphere (LNS) suspension (1.0 mg/mL) was obtained.

2.3. Modification of magnetic SiO₂ microspheres (Fe₃O₄@SiO₂-Cl)

2.7 g Fe₂(SO₄)₃, 7.2 g NaAc and 2.0 g PEG-4000 were dissolved in 80 mL EG and stirred for 30 min to completely dissolve them. Then the obtained solution was poured into the reaction kettle of polytetrafluoroethylene liner and it was placed in an electric blast drying oven for 8 hours at 200 °C. Fe₃O₄ NPs was collected from the solution using a magnet, washed several times with deionized water and ethanol, and dried in a vacuum drying oven. Then, 3.0 g Fe₃O₄ NPs was dispersed into 300 mL mixed solution of ethanol and deionized water with the volume ratio of 4:1 by ultrasonic treatment for 20 min. Next, 7 mL ammonia aqueous solution (25 wt%) was added to the above mixture solution and stirred vigorously for 15 min. Further, 14 mL TEOS was dropped slowly into through a constant pressure funnel and stirred mechanically for 8 h. The final product (Fe₃O₄@SiO₂) was separated from the reaction mixture using a magnet, washed with ethanol and deionized water, and dried at 80 °C. Finally, 3.0 g Fe₃O₄@SiO₂ was dispersed into 250 mL dry toluene by ultrasonic treatment for 20 min. Next 12 mL CPTES was slowly dropped slowly into through a constant pressure funnel and the suspension was placed on an oil bath under reflux at 110 °C for 24 h. The final product (Fe₃O₄@SiO₂-Cl) was separated from the reaction mixture using a magnet, washed with absolute ethanol, and dried under vacuum conditions at 100 °C for 24 h.

2.4. Preparation of magnetic lignin microspheres (Fe₃O₄@SiO₂-LNS)

1.0 g Fe₃O₄@SiO₂-Cl was added into 200 mL dry toluene by ultrasonic treatment for 20 min. Then 50 mL the as-prepared LNS suspension (1.0 mg/mL) was added to the above mixture solution and continued to disperse for 10 min. Next, the pH of the mixture was adjusted to 10.0 with 1.0 M NaOH solution, and the mixture was placed on an oil bath under reflux at 80 °C for 12 h. The final product (Fe₃O₄@SiO₂-LNS) was separated from the reaction mixture using a magnet, washed with ethanol and deionized water, and dried under vacuum conditions at 50 °C for 24 h.

2.5. Characterization

The morphology of the sample was determined by SU1510 scanning electron microscope of Hitachi Company and Phenom proX scanning electron microscope of the Netherlands Phenom-World, the chemical composition of the sample was characterized by 8400S Fourier Transform infrared spectrometer of Shimadzu Company, Japan, and the crystal structure of the sample was analyzed by Ultima IV X-ray diffraction analyzer of Kuraray Company. Micromeritics ASAP2020 Plus HD88 surface characteristics analyzer to characterize the surface characteristics of the sample.

2.6. Adsorption experiments

The effects of solution pH, adsorbent amount, adsorption time, initial dye concentration and temperature on the adsorption effect of Fe₃O₄@SiO₂-LNS on MB and RhB were investigated by single factor experiment. 50 mL dye of a certain concentration and a certain mass of Fe₃O₄@SiO₂-LNS were added into 100 mL conical flask, and the pH value of the solution was adjusted with 0.1 M NaOH solution and 0.1 M HCl solution. Then sealing the conical flask, shake it in a table constant temperature shaker at a certain temperature. After adsorption for a certain time, the adsorbent was separated with magnets, and the absorbance of the supernatant was measured by UV-2600 ultraviolet-visible spectrophotometer at the maximum wavelength of MB and RhB (664 nm and 554 nm), and the residual concentration of dye after adsorption was calculated using the standard curve. In accordance with formulas (1) and (2), the adsorption capacity (q_e, mg/g) and removal rate (R, %), respectively, of Fe₃O₄@SiO₂-LNS to MB and RhB were calculated.

$$q_e = \frac{(C_0 - C_e)V}{m} \quad (1)$$

$$R = \frac{C_0 - C_e}{C_0} \times 100\% \quad (2)$$

where C₀ is the initial concentration of dye, mg/L; C_e is the equilibrium concentration of the solution after adsorption, mg/L; V is the volume of solution, L; m is the mass of adsorbent, g.

2.7. Cyclic regeneration experiment

In order to study the reusability of $\text{Fe}_3\text{O}_4@\text{SiO}_2\text{-LNS}$ adsorbent, the used adsorbent was desorbed and used in the adsorption experiment again. 4 g/L $\text{Fe}_3\text{O}_4@\text{SiO}_2\text{-LNS}$ was added to 50 mL dye with a concentration of 60 mg/L. After adsorption for 360 min, $\text{Fe}_3\text{O}_4@\text{SiO}_2\text{-LNS}$ was separated from the dye solution by magnet, and the adsorption capacity was calculated. Then, the recovered $\text{Fe}_3\text{O}_4@\text{SiO}_2\text{-LNS}$ was put into 50 mL hydrochloric acid solution with pH=2.0. After sealing the sample bottle, the sample was placed in shaker at 25 °C for 24 h for desorption. Then, the dye was adsorbed three times under the same adsorption conditions mentioned above, and the regeneration efficiency r_e was calculated according to formulas (3).

$$r_e = \frac{q_n}{q_0} \times 100\% \quad (3)$$

where, q_0 (mg/g) is the first adsorption equilibrium adsorption capacity, and q_n (mg/g) is the adsorption equilibrium adsorption capacity.

3. Results and discussion

3.1. Characterization of lignin-based adsorbents

3.1.1 Morphology analysis

In this paper, lignin nanospheres (LNS) were firstly prepared through solvent-antisolvent method with tetrahydrofuran and water, and its morphology characterization were presented as Fig. 1(a).

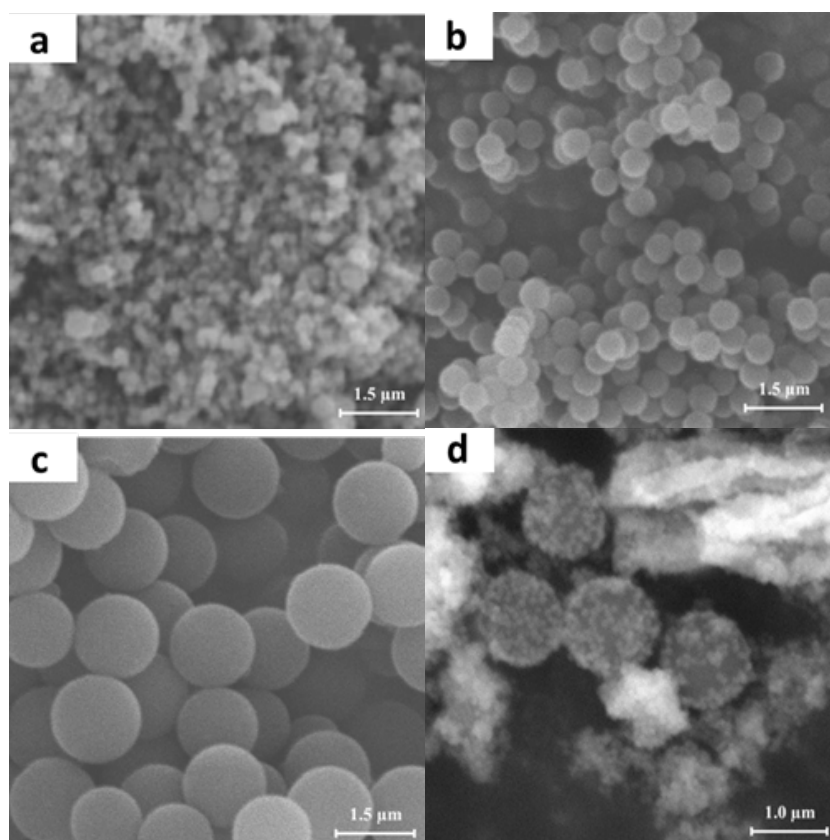


Fig. 1. The SEM images of (a) LNS, (b) Fe_3O_4 , (c) $\text{Fe}_3\text{O}_4@\text{SiO}_2$, and (d) $\text{Fe}_3\text{O}_4@\text{SiO}_2\text{-LNS}$.

It could be seen that LNS presented uniformly spherical shape with average size of 80.2nm and narrow size distribution. As shown in Fig. 1(b), the Fe_3O_4 nanoparticles, synthesized by

solvothermal methods, had a strong agglomeration phenomenon, due to the large specific surface area which resulted in the unstable state of surface energy, and the intermolecular force, hydrogen bond, static electricity, and other forces[14]. Coating with SiO₂ through sol-gel method, Fe₃O₄@SiO₂ showed smooth surface and improved dispersion as shown in Fig. 1(c). When Fe₃O₄@SiO₂ particles were loaded with LNS, it could be obviously seen that the lignin was located on the surface uniformly.

3.1.2. Elemental analysis

In order to further confirm the successful loading of LNS on the surface of Fe₃O₄@SiO₂-LNS, the element analysis of Fe₃O₄@SiO₂-LNS was carried out. The results in Fig. 2 showed that the major element is carbon, which accounted for about 51.0%, followed with oxygen (40.1%), silicon (7.1%), and ferrum (1.0%), indicating that not only lignin crosslinked with SC but also LNS located on the surface of the adsorbents.

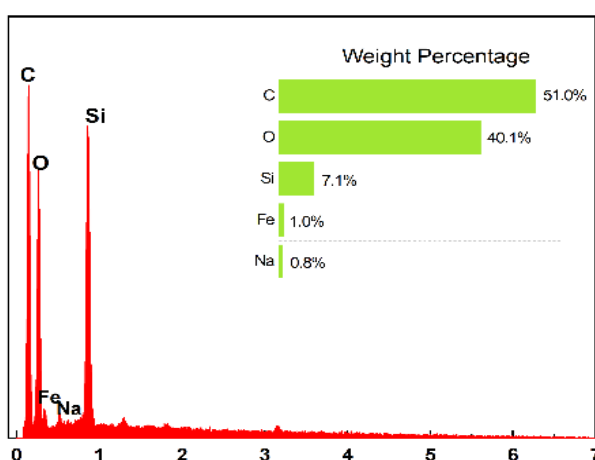


Fig. 2. EDS of Fe₃O₄@SiO₂-LNS.

3.1.3. Chemical structure analysis

Infrared spectroscopy was employed to analyze the structure of the alkaline lignin, modified lignin as shown in Fig. 3(a). The comparatively stronger signal peaks at 2920 cm⁻¹ and 2850 cm⁻¹ which corresponded to the -CH₃ and -CH₂ mainly from stearyl chloride, indicating the successful modification of lignin by stearyl chloride. Typical signal peaks of the lignin benzene ring structure at 1602, 1508, 1420 cm⁻¹ could be seen for both AL and SCAL. In addition, the characteristic absorption peaks corresponding to phenolic hydroxyl and alcohol hydroxyl of AL were at 1215 cm⁻¹, 1152 cm⁻¹ and 1085 cm⁻¹, and these three absorption peaks in SCAL were weakened, while the corresponding ester absorption peaks at 1200 cm⁻¹ were enhanced, indicating that some hydroxyl groups in SCAL had undergone esterification reactions [18].

Comparing the infrared spectra of Fe₃O₄ and Fe₃O₄@SiO₂ shown in Fig. 3(b), the absorption peak at 1093 cm⁻¹ due to the telescopic vibration peak of Si-O-Si bond and the absorption peak at 798 cm⁻¹ induced by Si-O bond were detected, which indicated that SiO₂ coating did not change the Fe-O skeleton of Fe₃O₄ [19], and meanwhile provided a bridging role between Fe₃O₄ and LNS. Since in the spectrum of Fe₃O₄@SiO₂-LNS, the typical stretching vibration peak at 578 cm⁻¹, which was attributed to the Fe-O bond in Fe₃O₄ nanoparticles was still found, but not existed in the spectrum of the lignin samples in Fig. 3(a), meaning that the lignin has been successfully loaded on Fe₃O₄. Moreover, the typical absorption peak at 1724 cm⁻¹ corresponding to the absorption peaks of carboxylate esters on benzene ring, and 1602 cm⁻¹, 1508 cm⁻¹ and 1460 cm⁻¹ from benzene ring on lignin were also detected.

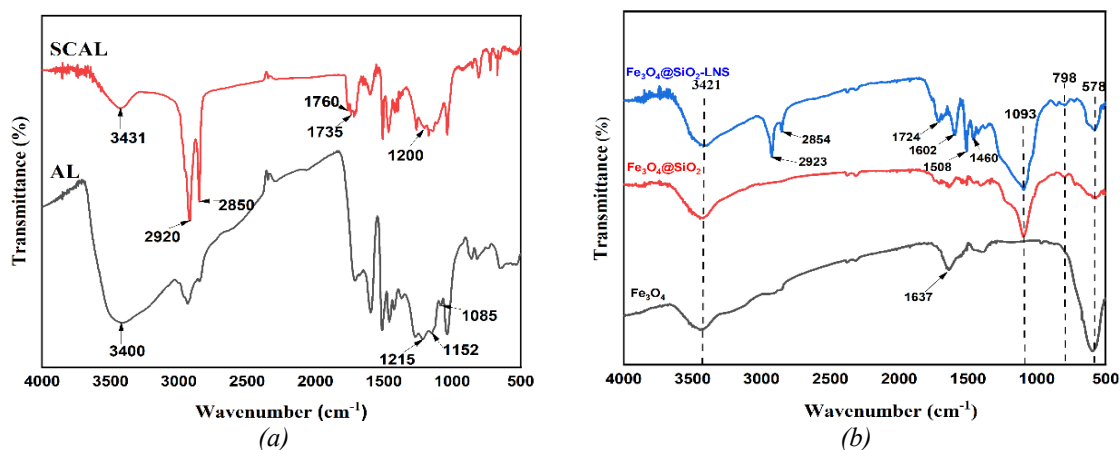


Fig. 3. Infrared spectrum of (a) AL and SCAL, (b) Fe_3O_4 , $\text{Fe}_3\text{O}_4@\text{SiO}_2$ and $\text{Fe}_3\text{O}_4@\text{SiO}_2\text{-LNS}$.

3.1.4. XRD analysis

X-ray diffraction (XRD) was employed to investigate the phase and crystal structure differences among Fe_3O_4 and lignin-based samples. As shown in Fig. 4, compared with Fe_3O_4 , a wide amorphous dispersion peak of SiO_2 was observed near 25° in the XRD spectra of $\text{Fe}_3\text{O}_4@\text{SiO}_2$, indicating that SiO_2 was coated on the surface of Fe_3O_4 particles. Similar diffraction peaks at 18.28° , 30.44° , 35.54° , 43.28° , 54.67° , 57.44° and 62.68° , indexed to (111), (220), (311), (400), (422), (511) and (440) planes of the inverse spinel face-centered cubic structure of Fe_3O_4 were found in the XRD spectrum of Fe_3O_4 , $\text{Fe}_3\text{O}_4@\text{SiO}_2$ and $\text{Fe}_3\text{O}_4@\text{SiO}_2\text{-LNS}$, indicating that there were little damage on the crystal structures of Fe_3O_4 during the coating the SiO_2 and LNS [20]. Besides, the typical diffraction peak of amorphous lignin appeared around 20° in XRD diagram of LNS[21].

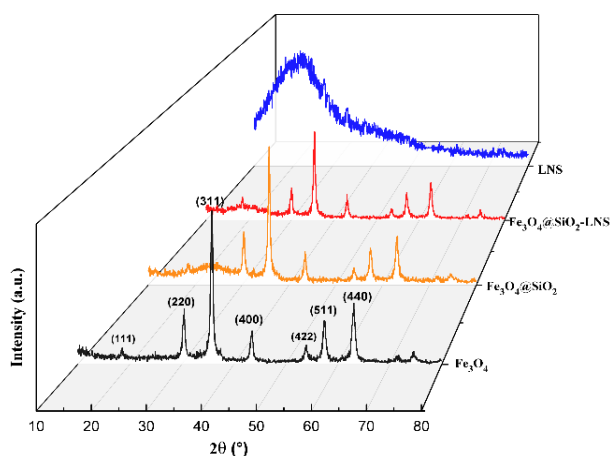


Fig. 4. XRD spectra of Fe_3O_4 and lignin-based samples.

3.1.5. Analysis of pore structure and specific surface area

Fig. 5(a) showed the N_2 adsorption and desorption isotherms of AL, LNS and $\text{Fe}_3\text{O}_4@\text{SiO}_2\text{-LNS}$. It could be clearly seen that AL has little response for the gas adsorption and desorption, indicating that the original lignin samples had strong coagulation and formed solid-state. However, when lignin samples were chemically changed to nano-size particles, its adsorption desorption isotherms exhibited IV type with H_3 hysteresis loop, since it rose rapidly in higher P/P_0 and the adsorption hysteresis loops were generated, indicating that there were rich mesoporous pores in the structure of LNS. Similarly, adsorption desorption isotherm of $\text{Fe}_3\text{O}_4@\text{SiO}_2\text{-LNS}$ also belonged to

IV type. Based on this, we calculated the specific surface area, total pore volume and average pore diameter and results were concluded in Table 1. As shown, compared with LNS, the specific surface area of $\text{Fe}_3\text{O}_4@\text{SiO}_2\text{-LNS}$ had a great decrease after loading on $\text{Fe}_3\text{O}_4@\text{SiO}_2$. However, the total pore volume increased largely mainly due to the space distance among the $\text{Fe}_3\text{O}_4@\text{SiO}_2$ particles, which could also be evidenced by the results of average pore diameter, 22.60nm.

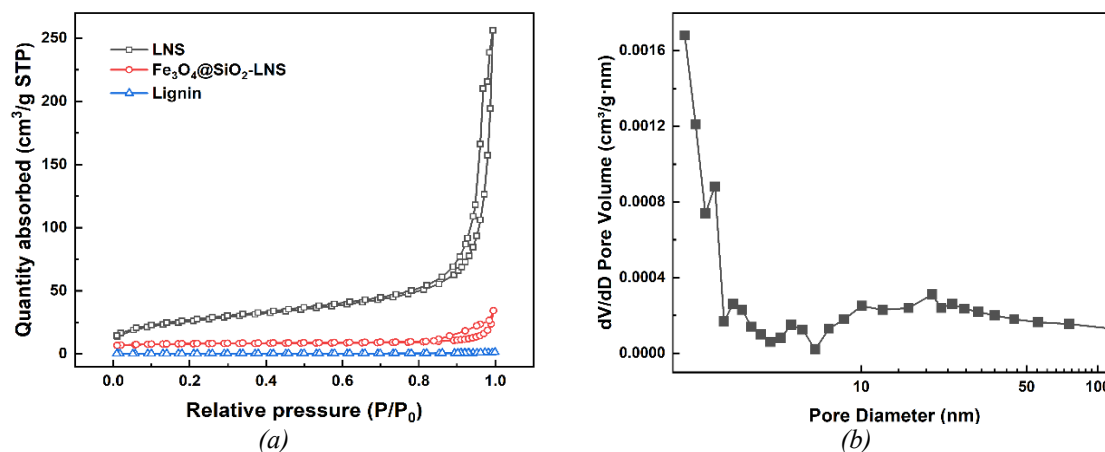


Fig. 5. (a) N_2 isothermal adsorption-desorption curve of Lignin, LNS and $\text{Fe}_3\text{O}_4@\text{SiO}_2\text{-LNS}$; (b) pore size distribution curve of $\text{Fe}_3\text{O}_4@\text{SiO}_2\text{-LNS}$.

Table 1. Pore structure and specific surface area of Lignin, LNS and $\text{Fe}_3\text{O}_4@\text{SiO}_2\text{-LNS}$.

Samples	Specific surface area ($\text{m}^2\cdot\text{g}^{-1}$)	Total pore volume ($\text{cm}^3\cdot\text{g}^{-1}$)	Average pore diameter (nm)
Lignin	0.31	0.0074	1.75
LNS	91.88	0.0105	2.72
$\text{Fe}_3\text{O}_4@\text{SiO}_2\text{-LNS}$	8.04	0.1321	22.60

3.2. Adsorption properties of $\text{Fe}_3\text{O}_4@\text{SiO}_2\text{-LNS}$

3.2.1. Effect of pH

The pH value of solution is one of the most important factors affecting the adsorption performance. As shown in Fig. 6(a), the adsorption performance was comparatively poor especially when $\text{pH} < 4$, since the electronegativity of $\text{Fe}_3\text{O}_4@\text{SiO}_2\text{-LNS}$ was comparatively low as shown in Fig. 6(b), resulting in weak electrostatic attraction force between adsorbents and dyes. Nevertheless, the adsorption capacity of $\text{Fe}_3\text{O}_4@\text{SiO}_2\text{-LNS}$ for MB and RhB increased with the increase of pH value, and the best adsorption condition for were both in alkaline environment. For RhB, the optimum pH was 9.72, at which the adsorption capacity reached the maximum, 13.48 mg/g. When pH increase to 11.26, the adsorption capacity decreased greatly, since the carboxyl groups in RhB were completely transformed into COO^- [33], leading to the increase of the electrostatic repulsion between RhB and $\text{Fe}_3\text{O}_4@\text{SiO}_2\text{-LNS}$ and the decrease of the adsorption capacity. However, the MB removal efficiency was kept improving with the increase of pH due to the less competitive hydrogen ion in aqueous solution, more negative adsorption sites on $\text{Fe}_3\text{O}_4@\text{SiO}_2\text{-LNS}$ (Fig. 6(b)) and the stronger electrostatic attraction between adsorbents and MB.

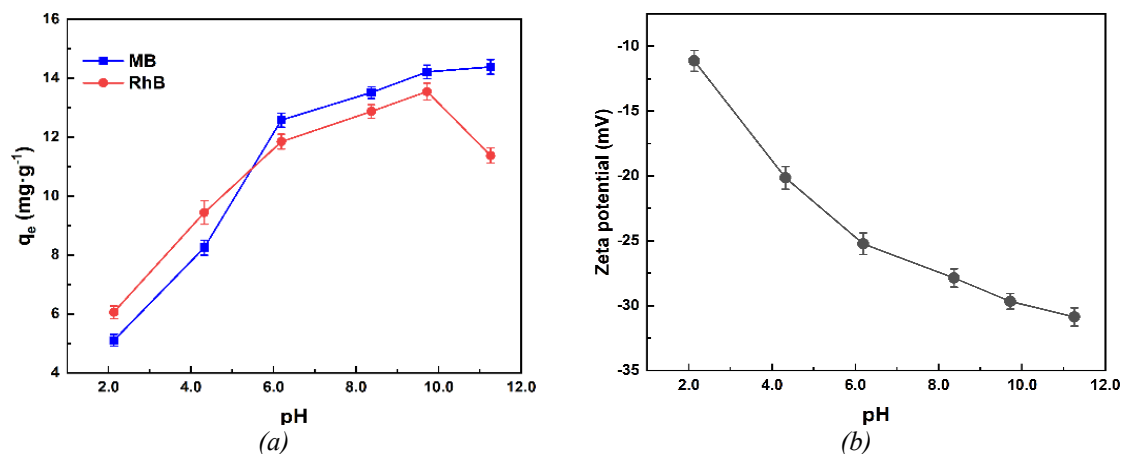


Fig. 6 (a) The adsorption capacity (q_e) of $\text{Fe}_3\text{O}_4@\text{SiO}_2\text{-LNS}$ for MB and RhB at different pH values, (b) Zeta potential of $\text{Fe}_3\text{O}_4@\text{SiO}_2\text{-LNS}$ at different pH values.

Note: Initial concentration of MB and RhB: 60 mg/L, dosage of $\text{Fe}_3\text{O}_4@\text{SiO}_2\text{-LNS}$: 4 g/L, temperature 313K.

3.2.2. Effect of adsorbent dosage

The adsorption capacity and removal efficiency of $\text{Fe}_3\text{O}_4@\text{SiO}_2\text{-LNS}$ for MB and RhB under different adsorbent dosage was also investigated as shown in Fig. 7. It could be obtained that the removal rate of MB and RhB could achieve above 90% at dosage of 2 g/L and 4 g/L respectively. With the increasing of adsorbent dosage, the removal efficiency was enhanced since the number of the corresponding active adsorption sites also increased. It was worth noting that the removal efficiency of $\text{Fe}_3\text{O}_4@\text{SiO}_2\text{-LNS}$ to MB was always higher than that of RhB under the same amount of adsorbent, possibly because the molecular size of MB is smaller than RhB, resulting in smaller steric hindrance from $\text{Fe}_3\text{O}_4@\text{SiO}_2\text{-LNS}$ and therefore more conducive to adsorption [22].

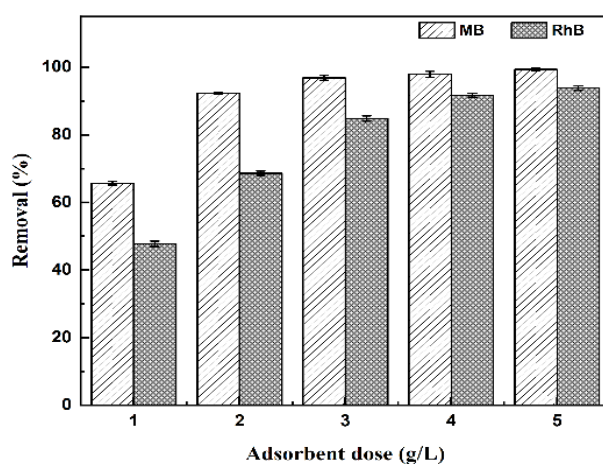


Fig. 7. The adsorption capacity (q_e) and removal efficiency of $\text{Fe}_3\text{O}_4@\text{SiO}_2\text{-LNS}$ for MB and RhB under different adsorbent dosage.

Note: Initial concentration of MB and RhB: 60 mg/L, temperature 313K, MB adsorption pH=11.0, RhB adsorption pH=9.5.

3.2.3. Effect of adsorption time

As could be seen from Fig. 8, during the first 90 min, the adsorption capacity of $\text{Fe}_3\text{O}_4@\text{SiO}_2\text{-LNS}$ for MB and RhB has a fast increase to about 12.2 mg/g and 10.9 mg/g, corresponding to removal rate of 81.3% and 72.7% respectively, indicating that the adsorption active

sites on lignin could provide a fast response for quantitative dye removal under suitable process conditions. Following, the adsorption process entered the stage of slow increase to saturation point.

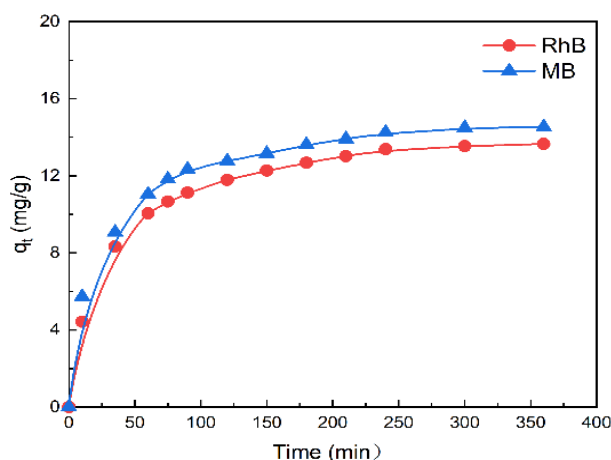


Fig. 8. Adsorption capacity of $Fe_3O_4@SiO_2-LNS$ for MB and RhB with different adsorption time. Note: Initial concentration of MB and RhB: 60 mg/L, dosage of $Fe_3O_4@SiO_2-LNS$ 4 g/L, temperature 313K, MB adsorption pH=11.0, RhB adsorption pH=9.5.

3.2.4. Effect of process temperature

As could be seen from Fig. 9, as the initial concentration of dye increased, the adsorption capacity, q_e , of $Fe_3O_4@SiO_2-LNS$ for MB and RhB was enhanced with fast- and slow-increasing tendency. More importantly, it was also clearly evidenced that the raising adsorption temperature could boost the capacity. However, as shown in Fig. 9(a), the upgrading rate of adsorption capacity for MB from 313K to 323K was lower than that from 303K to 313K, but this was not found in the RhB adsorption process shown in Fig. 9(b).

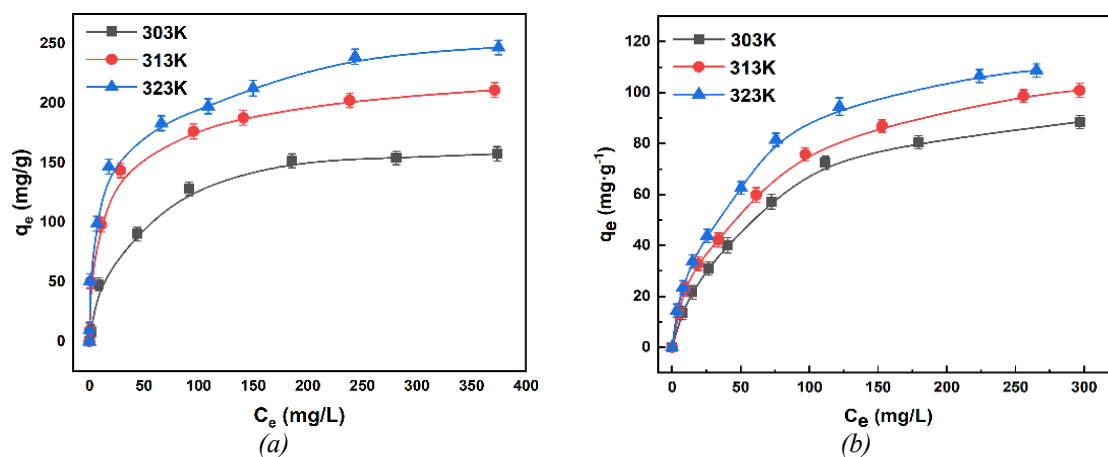


Fig. 9 The isothermal adsorption curve of $Fe_3O_4@SiO_2-LNS$ at 303 ~323k for (a) MB, (b) RhB ($Fe_3O_4@SiO_2-LNS$ dosage is 4 g/L, MB adsorption pH=11.0, RhB adsorption pH=9.5.)

In this paper, the adsorption process performance under different temperatures was also studied.

3.3. Adsorption mechanism

3.3.1. Adsorption thermodynamics

The changes of Gibbs free energy (ΔG , $\text{kJ}\cdot\text{mol}^{-1}$), enthalpy (ΔH , $\text{kJ}\cdot\text{mol}^{-1}$) and entropy (ΔS , $\text{J}\cdot\text{mol}^{-1}\cdot\text{K}^{-1}$) at different temperatures were calculated by using Van der Hoff and Gibbs-Helmholtz equations [23]. The influence of temperature was further investigated on adsorption process. The specific formula is as follows:

$$k = \frac{q_e}{C_e} \quad (4)$$

$$\Delta G^0 = -RT \ln k \quad (5)$$

$$\ln k = -\frac{\Delta H^0}{RT} + \frac{\Delta S^0}{R} \quad (6)$$

where q_e is the adsorption capacity at adsorption equilibrium ($\text{mg}\cdot\text{g}^{-1}$), C_e is the concentration of residual adsorbent at adsorption equilibrium ($\text{mg}\cdot\text{L}^{-1}$), R is the gas constant, $8.314 \text{ J}\cdot\text{mol}^{-1}\cdot\text{K}^{-1}$; T is the absolute temperature, K ; and k is the equilibrium constant, $\text{L}\cdot\text{g}^{-1}$. At different temperatures, q_e could be linearly fitted by $\ln(q_e/C_e)$, and the intercept was $\ln k$. k was substituted into Formula (5) to calculate ΔG . The slope and intercept of the line obtained by plotting $1/T$ by $\ln k$ were ΔH and ΔS . Results are shown in Table 2.

Table 2. Thermodynamic fitting parameters of $\text{Fe}_3\text{O}_4 @ \text{SiO}_2\text{-LNs}$ adsorbed dyes.

	T/K	303.15	313.15	323.15
MB	$\Delta G^0(\text{kJ}\cdot\text{mol}^{-1})$	-4.784	-5.462	-6.172
	$\Delta H^0(\text{kJ}\cdot\text{mol}^{-1})$	16.250		
	$\Delta S^0(\text{kJ}\cdot\text{mol}^{-1}\cdot\text{K}^{-1})$	0.069		
RhB	$\Delta G^0(\text{kJ}\cdot\text{mol}^{-1})$	-2.519	-3.122	-3.490
	$\Delta H^0(\text{kJ}\cdot\text{mol}^{-1})$	12.242		
	$\Delta S^0(\text{kJ}\cdot\text{mol}^{-1}\cdot\text{K}^{-1})$	0.049		

The ΔS^0 of $\text{Fe}_3\text{O}_4 @ \text{SiO}_2\text{-LNS}$ adsorbent for MB and RhB adsorption process were both greater than 0, indicating that the increases in the randomness at the solid-liquid interface during the adsorption process. The ΔG^0 was less than 0, and the absolute value of ΔG^0 increased with the increase of temperature, indicating that the adsorption process was spontaneous, and the increase of temperature was conducive to adsorption, which was consistent with the deduced results of Langmuir model. The ΔH^0 of the adsorption reaction was greater than 0, indicating that the adsorption process of $\text{Fe}_3\text{O}_4 @ \text{SiO}_2\text{-LNS}$ to MB and RhB was endothermic process. Studies showed that when the absolute value of ΔG^0 was less than $20 \text{ kJ}\cdot\text{mol}^{-1}$ [24, 25], physical adsorption existed in the adsorption process, and when ΔH^0 was within the range of $2\sim 29 \text{ kJ}\cdot\text{mol}^{-1}$, the force between the adsorbent and the solute was dominated by hydrogen bonding. Table 2 showed that the absolute values of ΔG^0 were less than $20 \text{ kJ}\cdot\text{mol}^{-1}$ and ΔH^0 were within the range of $2\sim 29 \text{ kJ}\cdot\text{mol}^{-1}$. Results showed a physical adsorption in the adsorption process of $\text{Fe}_3\text{O}_4 @ \text{SiO}_2\text{-LNS}$ on MB and RhB in addition to hydrogen bond.

3.3.2. Chemical structure changes

To verify the involved adsorption mechanism of $\text{Fe}_3\text{O}_4 @ \text{SiO}_2\text{-LNS}$, the chemical structure of $\text{Fe}_3\text{O}_4 @ \text{SiO}_2\text{-LNS}$ before and after adsorption were compared. It could be seen from Fig.10 that the aromatic ring stretching vibration peaks at 1600 cm^{-1} and 1512 cm^{-1} were shifted and the peaks also decreased. This indicated that there was $\pi\text{-}\pi$ interaction between the aromatic ring of lignin on $\text{Fe}_3\text{O}_4 @ \text{SiO}_2\text{-LNS}$ and the aromatic ring on the dye during the adsorption process [23, 26].

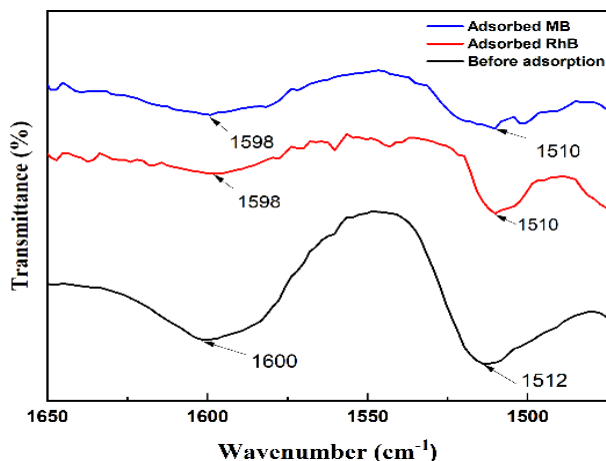


Fig. 10. Infrared spectrum of $\text{Fe}_3\text{O}_4@SiO_2$ -LNs before and after adsorption.

3.3.3. Mechanism speculation

Based on above characterization and adsorption kinetic modelling studies, the adsorption process of $\text{Fe}_3\text{O}_4@SiO_2$ -LNS on cationic dyes (MB, RhB) could be divided into three stages. Firstly, the dye particles diffused from the solution to the boundary layer of $\text{Fe}_3\text{O}_4@SiO_2$ -LNS with increasing disorder degree on the solid-liquid interface. In the second stage, MB and RhB particles were monolayer-adsorbed on $\text{Fe}_3\text{O}_4@SiO_2$ -LNS, resulting in rapid increasing adsorption capacity with time, mainly through the electrostatic interaction between the oxygen-containing functional groups of lignin and the amide nitrogen atoms in cationic dyes, π - π interaction between aromatic rings and hydrogen bond as shown in Fig. 11. Finally, the electrostatic repulsion between the surficial dye on $\text{Fe}_3\text{O}_4@SiO_2$ -LNS and the dissolved dye in solution resulted in the decrease of the adsorption rate and reaching equilibrium.

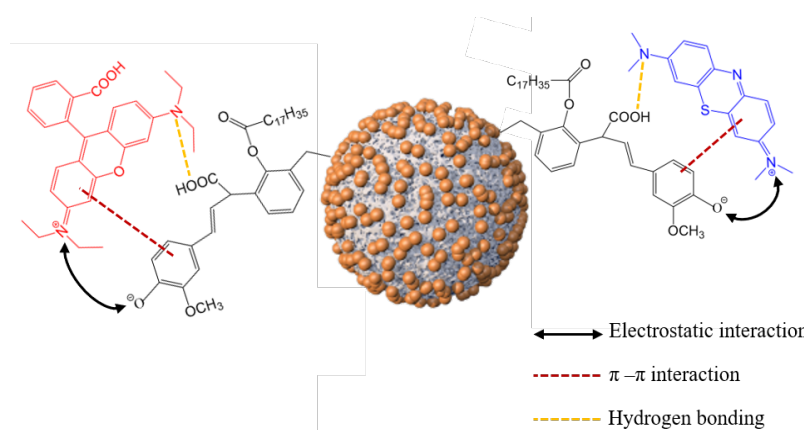


Fig. 11. Adsorption mechanism of $\text{Fe}_3\text{O}_4@SiO_2$ -LNS for MB and RhB.

3.4. Cycle regeneration

The regeneration ability of the absorbent affected its industrial applicability. In this paper, we used a pH-responsive mechanism (pH=2.0) for desorption to study the regeneration ability of $\text{Fe}_3\text{O}_4@SiO_2$ -LNS as shown in Fig. 12. As could be seen, after three-time regeneration cycles, the regeneration efficiency was still kept as 94.1% and 89.7% respectively, and the removal rate of $\text{Fe}_3\text{O}_4@SiO_2$ -LNS and primary adsorption only decreases by 5.9% and 10.7%, indicating that $\text{Fe}_3\text{O}_4@SiO_2$ -LNS had excellent recycling and regeneration ability, and could be used for multiple cycles of adsorption.

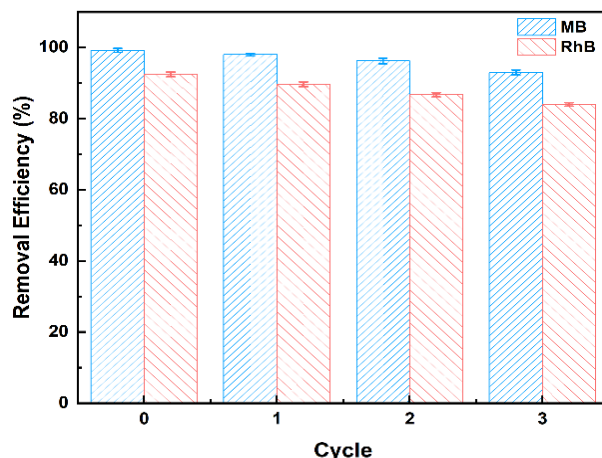


Fig. 12. The adsorbent recycling performance
(Initial concentration of dyes: 60 mg/L, dosage of $\text{Fe}_3\text{O}_4@\text{SiO}_2\text{-LNS}$: 4 g/L, temperature 313K, MB adsorption pH=11.0, RhB adsorption pH=9.5)

4. Conclusion

The Magnetic lignin microspheres $\text{Fe}_3\text{O}_4@\text{SiO}_2\text{-LNS}$ was successfully prepared and applied to adsorbing Methylene blue and Rhodamine B dyes. The results of adsorption experiments indicated that the adsorbent had good performance in alkaline solution. The kinetics and isotherm models show that the adsorption process is in accordance with the chemical adsorption of single molecular layer, and the maximum adsorption capacities were $258.40 \text{ mg}\cdot\text{g}^{-1}$ and $124.38 \text{ mg}\cdot\text{g}^{-1}$, respectively, which were higher than some dye adsorbents. Thermodynamic studies confirm that the adsorption process is a spontaneous endothermic reaction. Moreover, $\text{Fe}_3\text{O}_4@\text{SiO}_2\text{-LNS}$ adsorbent can be recycled, and the regeneration efficiency is over 85% after three cycles.

Acknowledgements

This research was funded by Provincial Natural Science Foundation of Zhejiang (Grant No. LTGS23C160001), the “Pioneer” and “Leading Goose” R&D Program of Zhejiang (Grant No. 2023C01195).

References

- [1] B. Du, Y. Bai, Z. Pan, Separation and Purification Technology 295 121302 (2022); <https://doi.org/10.1016/j.seppur.2022.121302>
- [2] J. Sharma, S. Sharma, V. Soni, Regional Studies in Marine Science 45 101802 (2021); <https://doi.org/10.1016/j.rsma.2021.101802>
- [3] A. M. Elgarahy, K. Z. Elwakeel, S. H. Mohammad, G. A. Elshoubaky, Cleaner Engineering and Technology 4 100209 (2021); <https://doi.org/10.1016/j.clet.2021.100209>
- [4] H. Tounsadi, Y. Metarfi, M. Taleb, K. E. Rhazi, Z. Rais, Ecotoxicology and Environmental Safety 197 110594 (2020); <https://doi.org/10.1016/j.ecoenv.2020.110594>
- [5] X. Jin, C. Wu, X. Tian, P. Wang, Y. Zhou, J. Zuo, Environmental Science and Ecotechnology 7 100110 (2021); <https://doi.org/10.1016/j.ese.2021.100110>
- [6] Y. H. Magdy, H. Altaher, Journal of Environmental Chemical Engineering 6(1), 834-841 (2018); <https://doi.org/10.1016/j.jece.2018.01.009>

- [7] N. Ghaemi P. Safari, Journal of Hazardous Materials 358 376-388 (2018); <https://doi.org/10.1016/j.jhazmat.2018.07.017>
- [8] K. Cui, B. Yan, Y. Xie, H. Qian, X. Wang, Q. Huang, Y. He, S. Jin H. Zeng, Journal of Hazardous Materials 350 66-75 (2018); <https://doi.org/10.1016/j.jhazmat.2018.02.011>
- [9] A. Kazzaz, Z. Feizi P. Fatehi, Green Chemistry 21(21), 5714-5752 (2019); <https://doi.org/10.1039/C9GC02598G>
- [10] B. M. Upton A. M. Kasko, Chemical Reviews 116(4), 2275-2306 (2015); <https://doi.org/10.1021/acs.chemrev.5b00345>
- [11] D. Mehta, S. Mazumdar S. K. Singh, Journal of Water Process Engineering 7 244-265 (2015); <https://doi.org/10.1016/j.jwpe.2015.07.001>
- [12] X. Li, Y. He, H. Sui L. He, Nanomaterials 8(3), 162 (2018); <https://doi.org/10.3390/nano8030162>
- [13] Y. Meng, C. Li, X. Liu, J. Lu, Y. Cheng, L. P. Xiao H. Wang, The Science of the Total Environment 685 847-855 (2019); <https://doi.org/10.1016/j.scitotenv.2019.06.278>
- [14] L. Fang, H. Wu, Y. Shi, Y. Tao Q. Yong, Frontiers in Bioengineering and Biotechnology 9 691528 (2021); <https://doi.org/10.3389/fbioe.2021.691528>
- [15] Y. Z. Ma, D. F. Zheng, Z. Y. Mo, R. J. Dong X. Q. Qiu, Colloids & Surfaces A Physicochemical & Engineering Aspects 559 226-234 (2018); <https://doi.org/10.1016/j.colsurfa.2018.09.054>
- [16] M. Faraji, M. Shirani H. Rashidi-Nodeh, TrAC Trends in Analytical Chemistry 141(1), 116302 (2021); <https://doi.org/10.1016/j.trac.2021.116302>
- [17] J. Zhou, Y. Liu, X. Zhou, J. Ren C. Zhong, Applied Surface Science 427 976-985 (2017); <https://doi.org/10.1016/j.apsusc.2017.08.110>
- [18] Y. Qian, Y. Deng, H. Li X. Qiu, Industrial & Engineering Chemistry Research 53(24), 10024-10028 (2014); <https://doi.org/10.1021/ie5010338>
- [19] E. B. Son, K. M. Poo, J. S. Chang K. J. Chae, Science of the Total Environment 615 161-168 (2018); <https://doi.org/10.1016/j.scitotenv.2017.09.171>
- [20] X. Jiang, Y. Zhao, X. Wang, L. Liu, Y. Wang, W. Zhang, L. Jiao W. Liang, Aqua(8), 738-753 (2018); <https://doi.org/10.2166/aqua.2018.051>
- [21] Z. Zhou, X. Peng, L. Zhong, X. Li R. Sun, Polymers 10(7), 724 (2018); <https://doi.org/10.3390/polym10070724>
- [22] L. A. Kang, Y. B. Liang, A. Jc A. Lz, Microporous and Mesoporous Materials 313 110840
- [23] H. N. Tran, S.-J. You H.-P. Chao, Journal of Environmental Management 188 322-336 (2017); <https://doi.org/10.1016/j.jenvman.2016.12.003>
- [24] S. Wei, W. Chen, Z. Tong, N. Jiang M. Zhu, Environmental Science and Pollution Research 28 51306-51320 (2021); <https://doi.org/10.1007/s11356-021-14324-4>
- [25] B. Zohre, S. Hashemi Yaser, H. Mahdi, A. Ali A. Mahvi Hosein, Water Science & Technology 74(5), 1235-1242 (2000)
- [26] K. Yang B. Xing, Chemical reviews 110(10), 5989-6008 (2010); <https://doi.org/10.1021/cr100059s>